FTIR Spectra and Normal-Mode Analysis of a Tetranuclear Mn Adamantane-like Complex in Two Electrochemically Prepared Oxidation States: Relevance to the Oxygen-evolving Complex of Photosystem II

Hendrik Visser,[†,‡] Christopher E. Dubé,[§,¶]

William H. Armstrong,[§,*] Kenneth Sauer,[†,‡,*] Vittal K. Yachandra[†,*]

Contribution from the [†]Melvin Calvin Laboratory, Physical Biosciences Division, Lawrence Berkeley National Laboratory, Berkeley, CA 94720; [‡]Department of Chemistry, University of California, Berkeley, CA 94720-5230; [§]Department of Chemistry, Eugene F. Merkert Chemistry Center, Boston College, Chestnut Hill, MA 02167-3860

[¶]*Present address: Charles Stark Draper Laboratory, 555 Technology Square, MS 37, Cambridge, MA 02139*

[*]*To whom correspondence should be addressed. E-mail: Armstrow@bc.edu, KHSauer@lbl.gov, or VKYachandra@lbl.gov*

Abbreviations: FTIR, Fourier transform infrared; ATR, attenuated total reflection; MCT, mercury cadmium telluride; bpea, *N*,*N*-bis(2-pyridylmethyl)ethylamine; tacn, 1,4,7-triazacyclononane; $HB(pz)_3^-$, hydrotris(1-pyrazolyl)borate; PS II, photosystem II; OEC, oxygen evolving complex; SCE, saturated calomel electrode; TBA, *t*-butylammonium

Abstract

The IR spectra and normal-mode analysis of the adamantane-like compound $[Mn_4O_6(bpea)_4]^{n+}$ in two oxidation states, $Mn^{IV}{}_4$ and $Mn^{III}Mn^{IV}{}_3$, that are relevant to the oxygen-evolving complex of photosystem II are presented. Mn–O vibrational modes are identified with isotopic exchange, $^{16}O \rightarrow {}^{18}O$, of the mono-μ-oxo bridging atoms in the complex. IR spectra of the $Mn^{III}Mn^{IV}{}_3$ species are obtained by electrochemical reduction of the $Mn^{IV}{}_4$ species using a spectroelectrochemical cell, based on attenuated total reflection [Visser et al. *Anal Chem* **2001**, *73*, 4374-4378]. A novel method of subtraction is used to reduce background contributions from solvent and ligand modes, and the difference and double-difference spectra are used in identifying Mn–O bridging modes that are sensitive to oxidation state change. Two strong IR bands are observed for the $Mn^{IV}{}_4$ species at 745 and 707 cm^{-1} and a weaker band at 510 cm^{-1}. Upon reduction, the $Mn^{III}Mn^{IV}{}_3$ species exhibits two strong IR bands at 745 and 680 cm^{-1}, and several weaker bands are observed in the 510 - 425 cm^{-1} range. A normal mode analysis is performed to assign all the relevant bridging modes in the oxidized $Mn^{IV}{}_4$ and reduced $Mn^{III}Mn^{IV}{}_3$ species. The calculated force constants for the $Mn^{IV}{}_4$ species are $f_{r^{IV}}$ = 3.15 mdyn/Å, f_{rOr} = 0.55 mdyn/Å, and f_{rMnr} = 0.20 mdyn/Å. The force constants for the $Mn^{III}Mn^{IV}{}_3$ species are $f_{r^{IV}}$ = 3.10 mdyn/Å, $f_{r^{III}}$ = 2.45 mdyn/Å, f_{rOr} = 0.40, and f_{rMnr} = 0.15 mdyn/Å. This study provides insights for the identification of Mn–O modes in the IR spectra of the photosynthetic oxygen-evolving complex during its catalytic cycle.

Introduction

The world's supply of oxygen is a by-product of the water oxidation process carried out by oxygenic photosynthesis in organisms such as cyanobacteria and green plants. Water oxidation takes place in a trans-membrane protein cluster, photosystem II (PS II), where it is catalyzed by the oxygen-evolving complex (OEC). A photon-induced electron abstraction from the OEC occurs during each of the four state transitions of the catalytic cycle ($S_0 \rightarrow S_1$, $S_1 \rightarrow S_2$, $S_2 \rightarrow S_3$, $S_3 \rightarrow [S_4] \rightarrow S_0$).[1] Dioxygen is released when the S_3 state returns to the S_0 state, via the hypothesized S_4 state.

Although progress has been made in obtaining a crystal structure of PS II,[2] most of our electronic and structural knowledge about the OEC has been obtained from X-ray absorption[3-5] and EPR spectroscopy.[6-9] From these studies, it is known that the OEC contains four manganese atoms which are arranged in two or three di-μ-oxo moieties and one mono-μ-oxo moiety. In addition, co-factors Ca^{2+} and Cl^- are required for water oxidation.[10] One or two histidines are directly ligated to one of the manganese atoms of the OEC, and water has also been implicated as a ligand of Mn.[11-14] Glutamate and aspartate are thought to provide most of the other ligands.[10,15] During each of the first two state transitions ($S_0 \rightarrow S_1$, $S_1 \rightarrow S_2$) an electron is abstracted from Mn.[16-19] However, during the third state transition ($S_2 \rightarrow S_3$) X-ray spectroscopy studies indicate that oxidation of manganese is unlikely; an electron may instead be extracted from a ligand or a nearby residue.[16,17] The synthesis and study of a wide variety of manganese compounds have been critical for the interpretation of the X-ray and EPR spectra of the OEC.[20-29]

Several mechanisms of water oxidation have been proposed. These mechanisms are divided here into four groups, in which the character of the oxygen atoms that ultimately form dioxygen is different. In these four groups the oxygen atoms come from: two terminal oxygens bound to two separate manganese atoms,[4,12,16,28,30-35] one terminal oxygen and one oxygen not bound to the manganese cluster,[4,16,28,35-39] one terminal and one bridging oxygen,[28,35,40] or two μ-oxo bridges.[4,16,35,41,42] Each of these mechanisms involves distinctly different Mn–O bonds formed and broken during the catalytic cycle.[21] Therefore, it is useful to apply a technique, such as vibrational spectroscopy, that distinguishes among the different kinds of Mn–O bonds and other relevant bonds of the OEC.

Recently, vibrational spectroscopy has been added as an investigative tool to study the structure and mechanism of the OEC. Changes during the catalytic cycle in the 1800 - 1200 cm^{-1} range, which arise from vibrations of the protein-residues ligated to the OEC,[14,43-49] are complemented by those of the Mn–ligand vibrations, specifically the Mn–O vibrations, which occur in the 200 - 1000 cm^{-1} range.[49-52] Vibrations of a water molecule in the OEC have been detected in the 2500 - 3700 cm^{-1} range, using H/D exchange studies.[14,53] The low frequency range is especially helpful in determining the mechanism of water oxidation. Chu et al.[43,49,51] were able to obtain IR difference spectra of the $S_1 \rightarrow S_2$ transition of the OEC in the 350 - 1000 cm^{-1} range. They identified a Mn–O–Mn vibration at 625 cm^{-1} in the S_1 state, which shifts to 606 cm^{-1} in the S_2 state (596 cm^{-1} in the ^{18}O-treated sample). Low frequency (220 - 620 cm^{-1}) resonance Raman spectra of the OEC were obtained by Cua et al.[54] They observed two scattering peaks at 348 cm^{-1} and 476 cm^{-1} which are sensitive to isotopic exchange of D for H and were tentatively assigned to either a Mn–OH or Mn–OH_2 vibration. Such vibrational

assignments of the OEC are based on studies of known manganese compounds.[49,55-61]

Vibrational spectra of manganese model compounds are indispensable for the interpretation of the IR and Raman spectra of the OEC. There are several multinuclear Mn complexes that have been prepared to understand the spectral properties of the Mn complex in the OEC. An excellent summary of the low frequency vibrational modes observed in such complexes is presented in a review by Babcock and coworkers[49] (see also Results and Discussion). However, only a few manganese model compounds have been extensively studied by IR or Raman spectroscopy using isotopic exchange, such as $^{16}O \rightarrow {}^{18}O$,[23,56] and normal mode analysis.[62] Isotopic exchange is necessary to distinguish Mn–O vibrational modes from modes which involve other parts of the complex. Normal-mode analysis of the complexes is required to understand the pattern of the identified vibrations and to extract force constants. These force constants can be used to predict and analyze the vibrational spectra of other compounds and the OEC. The compounds for which the Mn-ligand force constants are known are various Mn oxide compounds (MnO_3X^{n-}, with X = O, F, or Cl),[63-65] Mn halide compounds ($Mn^{VI}X_4$, with X = Cl, Br, or I),[66,67] compounds that contain a Mn–oxygen ligand unit held by porphyrin derivatives,[68] and a mono-μ-oxo compound.[62] Only the last compound contains a moiety which is structurally relevant to the OEC. Therefore, more vibrational studies are needed of manganese compounds in different oxidation states relevant to the catalytic cycle of the OEC. It is not always possible to obtain solid homologous multinuclear Mn compounds in different oxidation states, but it is often possible to generate such redox states electrochemically in solution. Therefore, a technique which combines electrochemistry and IR spectroscopy has been utilized to advantage as described below.

In this paper we present the IR spectra and a normal-mode analysis of the tetranuclear adamantane-like Mn compounds $[Mn^{IV}_4O_6(bpea)_4]^{4+}$ (**1**) and $[Mn^{IV}_3Mn^{III}O_6(bpea)_4]^{3+}$ (**2**), with ^{16}O and ^{18}O in the bridging moiety, where bpea (*N*,*N*-bis(2-pyridylmethyl)ethylamine) is the terminal ligand (Figure 1).[69] The ligand bpea has one non-aromatic nitrogen (indicated by an asterisk in Figure 1) and two aromatic nitrogens ligated to Mn, which causes the compound to approach S_4 symmetry. The IR spectrum of **1** as a solid reveals a Mn–O–Mn stretch mode at 709 cm^{-1}, which shifts to 675 cm^{-1} upon ^{16}O to ^{18}O exchange.[69] This frequency is close to 730 cm^{-1}, which was identified as a Mn–O vibration for the structurally analogous $[Mn^{IV}_4O_6(tacn)_4]^{4+}$(**3**), where tacn is 1,4,7-triazacyclononane.[70] In contrast to bpea, tacn has three equivalent non-aromatic nitrogens ligated to Mn, with the compound close to T_d symmetry.

The bpea compound in acetonitrile has a reversible wave in the cyclic voltammogram at $E_{1/2}$ = 0.104 V versus SCE (Standard Calomel Electrode) for the ($Mn^{IV}_4 + e^- \rightleftarrows Mn^{III}Mn^{IV}_3$) redox couple. In the present work a novel attenuated total reflection (ATR) spectroelectrochemical cell[71] is used to obtain IR difference spectra of the adamantane-like compound in the two oxidation states. The reversibility of the redox couple is advantageously utilized to distinguish IR frequencies of the compound from non-reversible background signals. In addition, $^{16}O \rightarrow ^{18}O$ isotopic exchange is used to distinguish Mn–O bridging modes from the terminal ligand modes. This is the first time that such an IR study has been performed on a manganese compound in two oxidation states in solution relevant to the OEC, and a normal-mode analysis identifying the bridging Mn–O modes sensitive to the oxidation state of Mn

Experimental

Synthesis. Synthesis and isotopic exchange of the bridging oxygen atoms of **1** were performed as described in Dubé et al.,[69] where the counter ion is either Br^- (for the solid compound IR spectra) or ClO_4^- (for the acetonitrile solution IR difference spectra during electrochemistry). During the isotopic exchange a 90% replacement of ^{16}O by ^{18}O was achieved.[69]

Electrochemistry. A home-built spectroelectrochemical apparatus described in detail elsewhere[71] was used to measure the solution IR spectra of the redox species during electrochemistry. The apparatus consists of an electrochemical cell made of Teflon, which interfaces with an ASI DuraSamplIR™ (Applied Systems Inc., Annapolis, MD) ATR accessory.[72,73] The ATR device has a wide spectral range of 16,700 – 250 cm^{-1}, and a small opaque region of 2250 – 1900 cm^{-1}. Pt gauze was used for both the working and counter electrodes. The counter electrode was placed inside a glass tube fitted with a fritted glass disk to minimize diffusion of electrochemical products. The non-aqueous (CH_3CN, 0.1 M TBA(PF_6)) $Ag/AgClO_4$ reference electrode (determined to be 270 mV more positive than SCE) was isolated from the bulk solution by an additional electrolyte bridge (a glass tube fitted with a Vycor® tip), which was changed between samples to avoid contamination.

The electrolyte solution (0.1 M TBA(PF_6) in acetonitrile) was dried over Al_2O_3 and bubbled with Ar prior to each experiment. Sample solutions (0.8 mL) of either 2.8 mM $[Mn^{IV}_4\mathbf{^{16}O}_6(bpea)_4](ClO_4)_4$ or 2.5 mM $[Mn^{IV}_4\mathbf{^{18}O}_6(bpea)_4](ClO_4)_4$ were kept under a constant purge of Ar during electrochemistry. Ar gas was bubbled through dry acetonitrile (dried with Al_2O_3) to minimize evaporation and small changes in the concentration. Electrochemistry was performed

using a BAS CV-27 Voltammetry Controller. Reduction of the Mn^{IV}_4 complex was done at –0.7 V and oxidation at +0.3 V vs. the $Ag/AgClO_4$ reference electrode ($E_{1/2}$ = –0.2 V vs. $Ag/AgClO_4$, and +0.10 V vs. SCE[69]).

IR spectroscopy. A Bruker IFS88 FTIR spectrometer was used to collect the infrared data. The spectrometer contains a KBr beam-splitter and a broad band MCT detector (lower cut-off 400 cm^{-1}). KBr disks were used to obtain the IR spectra (averaged over 100 scans) of both the solid ^{16}O and ^{18}O adamantane-like $[Mn^{IV}_4O_6(bpea)_4]Br_4$ compounds, at a resolution of 1 cm^{-1}.

The solution IR spectra during the electrochemistry were taken at a resolution of 4 cm^{-1} and were recorded in rapid scan mode (128 ms per scan). The data collection protocol has been described previously[71] and is summarized here briefly (see Figure 2). The experiments were performed by alternating between reduction and oxidation conditions, enabling us to make a distinction between electrochemicaly reversible and non-reversible signals. Each experiment had a sequence of different redox steps; no potential applied (step 1), reduction (step 2), oxidation (step 3), reduction (step 4), oxidation (step 5). During the first redox step no potential is applied because the compound is already in the oxidized state. This sequence enables us to calculate two difference spectra during the reduction cycle of the Mn^{IV}_4 species (oxidized minus reduced), and two difference spectra during the oxidation cycle of the $Mn^{III}Mn^{IV}_3$ species (reduced minus oxidized).

During a reduction or oxidation step, 1600 scans were taken and collected into 16 separate groups (100 scans per group). Electrochemically reversible signals have successive maxima and minima in the signal intensity as a consequence of the redox sequence. Only the maxima and minima of the oscillating IR intensity are used to calculate the difference spectra, indicated by the thicker lines in Figure 2. The time profile of various IR signals during the

electrochemistry was studied to determine what groups need to be discarded. The averaged maximum and minimum spectra were subtracted from each other to obtain the difference spectra during the reduction and oxidation cycle respectively (Figure 2).

To enhance the signal-to-noise ratio of the difference spectra this redox sequence is repeated three times for each sample, ^{16}O and ^{18}O. The electrochemical solution is maintained after each redox sequence under oxidizing conditions for about 30 min to return the sample to the oxidized state. This conversion was not complete due to diffusion limitations; consequently, the IR difference signals of second and third redox sequence were smaller than for the first redox sequence. To correct for this difference in signal intensity the averaged reduction and oxidation spectra were calculated by weighting the spectra of each redox sequence by the intensity of the reversible 1030/1022 cm^{-1} difference signal. This corrected the differences in intensity due to the incomplete oxidation between experiments.

All of the difference spectra are presented such that features due to the oxidized species Mn^{IV}_4 are positive and those for the reduced species $Mn^{III}Mn^{IV}_3$ are negative. Therefore, reversible features have the same sign in the difference spectra during both the reduction and oxidation cycles, and non-reversible features have the opposite sign. When the averaged difference spectra from the reduction and oxidation cycle are added the non-reversible background signals are, in principle, eliminated and only the reversible features remain in the Sum spectrum (shown in Figures 4, 5, 6 and 8).

Normal-mode Analysis. Normal-mode analysis of the adamantane-like compound, which is described in detail elsewhere,[74] was performed using the *GF*-matrix method.[75] The linear algebra calculations of the normal-mode analysis were performed using Mathematica 3.0 (Wolfram Research). The frequencies of the normal modes were matched with the observed

frequencies by varying the force constants in steps of 0.05 mdyn/Å. The stretch force constants used for simulations of **1** are: (1) the stretching force constant of the Mn^{IV}–O bonds, $f_{r\,IV}$, and (2) the stretching coupling constants between two adjacent bonds with oxygen, f_{rOr}, or manganese, f_{rMnr}, at the apex. In the normal mode simulations of **2** the stretch force constant of the Mn^{III}–O bonds, $f_{r\,III}$, is also included.

Results and Discussion

FTIR spectra of the solid $[Mn^{IV}_4O_6(bpea)_4]^{4+}$ compound

Isotopic exchange of the bridging oxygen atoms is used to distinguish the predominant Mn–O vibrational modes of the adamantane-like compound from modes that do not involve oxygen atoms, such as vibrations of the terminal ligand bpea. The FTIR absorption spectra of the solid $[Mn^{IV}_4\mathbf{^{16}O}_6(bpea)_4]^{4+}$ (black) and $[Mn^{IV}_4\mathbf{^{18}O}_6(bpea)_4]^{4+}$ (red) compounds are shown in Figure 3. The isotope-sensitive vibrational modes are indicated by arrows. The most intense band in the spectrum of the ^{16}O compound is at 707 cm^{-1}, and a weaker band occurs at 510 cm^{-1}. These bands shift to 674 cm^{-1} and 490 cm^{-1}, respectively, in the ^{18}O spectrum.

Another Mn–O mode, detected as a shoulder at ~745 cm^{-1} in the ^{16}O absorption spectra, is not present in the ^{18}O spectrum. This transition is evident in the ^{16}O–^{18}O difference spectrum (blue curve in Figure 3). In the difference spectrum the shoulder at 745 cm^{-1} is a broad vibrational band which overlaps the 707/674 cm^{-1} difference signal. It is not obvious where the ^{18}O companion of this broad band appears. However, in the difference spectrum the 707 cm^{-1} signal has a smaller intensity than the 674 cm^{-1} signal. Upon isotopic exchange, only the frequency of vibrational modes is expected to change significantly, while the intensity of the transition only change minimally. Therefore, this change in signal intensity is an indication that

the ^{18}O companion of the 745 cm^{-1} peak is underneath the 707 cm^{-1}. Figure 4 shows that the difference signal around 700 cm^{-1} can be simulated by two ^{16}O-absorption bands at 745 cm^{-1} and 707 cm^{-1} (black curves), and two ^{18}O-absorption bands at 705 cm^{-1} and 674 cm^{-1} (red curves). This suggests that the 745 cm^{-1} mode shifts to 705 cm^{-1} upon isotopic exchange, and is underneath the ^{16}O species 707 cm^{-1} mode in the difference spectrum.

The 510/490 cm^{-1} difference signal is not strong enough to be clearly distinguished from the other signals due to the small differences in amounts of free bpea molecules, counter ions, and captured solvent molecules between the ^{16}O and ^{18}O solid samples. Only difference signals with strong intensity can be identified when the two solid compounds are compared.

A weak absorption band which is observed at about 1016 cm^{-1} for the ^{16}O compound, is not present in the ^{18}O compound. This vibrational mode could be the first overtone of the 510 cm^{-1} mode. However, the ^{18}O band of this overtone mode, expected to be near 980 cm^{-1}, is not seen. Therefore, the band observed at 1016 cm^{-1} is most likely not an overtone, but some contamination which occurred during the preparation procedure. All the other bands that do not shift upon the $^{16}O \rightarrow {}^{18}O$ exchange are due to vibrational modes of bpea, counter ions, and solvent molecules which are part of the crystals. Changes in intensity of absorption bands, such as at 1121, 1109, and 1097 cm^{-1}, are not due to isotopic exchange but due to small differences in amounts of free bpea molecules, counter ions, and solvent molecules between the ^{16}O and ^{18}O solid samples.

FTIR (oxidized, Mn^{IV}_4 – reduced, $Mn^{III}Mn^{IV}_3$) difference spectra of the adamantane-like compound in solution

Figures 5 and 6 show the FTIR (oxidized, Mn^{IV}_4 – reduced, $Mn^{III}Mn^{IV}_3$) solution difference spectra measured for the ^{16}O and ^{18}O compounds, respectively, using the spectroelectrochemical set-up[71] described in the experimental section. Each figure contains 3 spectra: the difference spectra during the reduction cycle (purple), the difference spectra from the oxidation cycle (blue), and the Sum spectra (black). Both figures are plotted so that features due to the Mn^{IV}_4 oxidation state have a positive intensity, while the features due to the $Mn^{III}Mn^{IV}_3$ oxidation state have a negative intensity. A distinction can be made between reversible and non-reversible signals by comparing the difference spectra collected during the reduction and oxidation cycles. Reversible signals have the same sign for the reduction and oxidation cycles, but non-reversible signals have opposite sign.

Figures 5 and 6 show non-reversible signals, indicated by ‡, at 1100 cm^{-1}, 917 cm^{-1}, 739 cm^{-1}, and 624 cm^{-1}, which are most likely due to decomposition of the electrolyte and solvent.[71] The signals indicated by an asterisk, at 877 cm^{-1}, 844 cm^{-1}, and 560 cm^{-1} in Figures 5 and 6 are non-reversible signals due to small changes in the concentration of the electrolyte anion PF_6^-.[71] The Sum spectra are obtained by adding the difference spectra from the reduction cycle and a fraction of difference spectra from the oxidation cycle (see Figure 2), in order to minimize the non-reversible electrolyte signals over the whole spectral range (400 - 4000 cm^{-1}, higher frequency data not shown). In the Sum spectra shown in Figures 5 and 6 the non-reversible signals are absent or reduced greatly in intensity.

Two different types of reversible signals, both sensitive to Mn oxidation state change, can be observed by comparing the Sum spectra in Figure 5 and 6. The first group of reversible

signals, indicated by black arrows, corresponds to modes that have the same energy position for the ^{16}O and ^{18}O difference-spectra. This is very clear when these spectra are directly compared in the top part of Figure 7, where the difference signals at 1162/1154 cm^{-1}, 1054/1048 cm^{-1}, 1030/1022 cm^{-1}, 773 cm^{-1}, 669/659 cm^{-1}, and at 541/528 cm^{-1} do not shift on $^{16}O \rightarrow ^{18}O$ exchange. These bands are clearly absent in the double-difference spectrum shown in the bottom part of Fig. 7, indicating that no bridging Mn–O modes are involved. These reversible signals are assigned to the changes in the vibrational modes of the terminal-ligand bpea, caused by the change in Mn–bpea interaction following a change in the Mn oxidation state.

The second, more important group of reversible signals sensitive to Mn oxidation state change, indicated by red arrows, is dependent on the isotopic state of the oxygens; therefore this indicates that bridging Mn–O modes are involved. Some of these signals are indicated by red arrows, such as the most dominant oxidized minus reduced difference signal at 709/680 cm^{-1}, which shifts to 677/653 cm^{-1} upon isotopic $^{16}O \rightarrow ^{18}O$ exchange. This shift is even more obvious in Figure 7, where Sum spectra from both the ^{16}O and ^{18}O compounds are compared (top part of Figure 7), and in the double-difference spectrum shown in blue in the bottom part of Figure 7.

Other weak reversible signals, sensitive to isotopic exchange, can be observed in the 520 - 425 cm^{-1} range in Figures 5 and 6. A positive feature is present at 510 cm^{-1} in Figure 5, which could be due to the Mn^{IV}_4 oxidation state, while a negative feature occurs at 493 cm^{-1} in the $Mn^{III}Mn^{IV}_3$ oxidation state. Complementary isotopically shifted peaks could be the positive feature at 493 cm^{-1} and the negative band at 471 cm^{-1} in Figure 6. A positive feature also appears at 446 cm^{-1} in Figure 5 that is not present in Figure 6.

A direct comparison of the ^{16}O and ^{18}O difference spectra in Figure 7 shows that several differences occur between the two spectra in the 520 - 425 cm^{-1} range. However, the signals are

weak and it is difficult to determine those that are reversible and sensitive to isotopic exchange in this region. To eliminate the non-isotopic sensitive signals the double-difference spectrum of the ^{16}O and ^{18}O difference spectra is shown in Figure 7. This exposes only the reversible signals sensitive to $^{16}O \rightarrow ^{18}O$ exchange. Two strong bands appear, a negative signal at 490 cm^{-1} and a positive signal at 448 cm^{-1}. Additionally some weaker double-difference signals appear between these two strong bands. This indicates that the features in the 520 - 425 cm^{-1} range contain Mn–O modes. However, additional information from the normal-mode analysis is needed to completely understand the changes observed in the ^{16}O and ^{18}O difference as well as the double-difference spectra in this region.

Normal-mode analysis

Several vibrational bands in the IR spectra of the adamantane-like compound are identified as Mn–O core modes, by isotopic $^{16}O \rightarrow ^{18}O$ exchange of the bridging oxygens. Some of these bands are sensitive to the oxidation state of the Mn atoms. Normal mode analysis aids the assignment of the observed bands and enables us to extract specific information about the Mn–O bonds.

The adamantane-like compound contains 146 atoms and has 432 vibrational modes. Since our primary interest is in the Mn–O bridging modes of the Mn_4O_6 core and only a limited number of bands can be identified, several approximations are required to perform a normal-mode analysis of compounds **1** and **2** (a more detailed discussion is given by Visser[74]). The terminal bpea ligand vibrational modes are assumed to be mostly independent of the Mn–O modes and are not included in the normal-mode analysis. In addition, the Mn–N(bpea) terminal ligand interactions, expected to be below 400 cm^{-1}, are much weaker than those of the bridging

Mn–O modes and, therefore, are not included in the normal-mode analysis. Previous studies using a dinuclear Mn mono-μ-oxo compound have shown that these assumptions are reasonable and good agreement is obtained between the observed and calculated modes.[62]

However, if the bpea and Mn–O vibrational modes interact, a small $^{16}O \rightarrow {}^{18}O$ isotopic effect is expected for the bpea modes. In the (oxidized – reduced) difference spectra reversible signals are observed which do not shift between the ^{16}O and ^{18}O spectra and which are absent in the ($^{16}O - {}^{18}O$) double-difference spectrum. This indicates that these modes are not sensitive to the $^{16}O \rightarrow {}^{18}O$ exchange. All of these difference signals are at positions that correspond to the vibrational modes of the terminal ligand, bpea (Figure 3). Therefore, it is concluded that these reversible signals are caused by changes in the bpea ligand upon a change in oxidation state of Mn. This supports the assumption that the modes of the terminal ligand bpea are not influenced by the Mn–O core, and can indeed be treated separately. As a result, the number of atoms considered is decreased to 10 and the number of vibrational modes to 24.

This collection consists of twelve stretching and twelve bending Mn–O modes. The bending modes are expected to be well below 400 cm^{-1}. Including bending modes in the calculations causes only small shifts in frequencies of the stretching modes.[74] These shifts can be corrected by small alterations of the stretching force constants, ~0.1 mdyn/Å. The corrections of the force constants are on the same order as the changes needed to optimize the calculated modes when a different overall symmetry is assumed. Therefore, omitting the bending force constants is reasonable, given the other approximations made for the normal-mode calculations.

Finally, some assumptions are required about the overall symmetry of the compound. If the influence of the terminal bpea ligand on **1** is ignored, T_d symmetry can be applied to the $Mn^{IV}{}_4O_6$ core of **1**. However, if bpea is included, the highest symmetry possible is S_4. The

highest possible symmetry of the $Mn^{IV}_3Mn^{III}O_6$ core of **2** is C_s, ignoring the influence of the bpea ligand. Including the bpea in the symmetry analysis reduces the symmetry to C_1, which is close to C_s symmetry. No normal-mode analysis was performed for the overall C_1 symmetry because no significant additional information is obtained by including the C_1 symmetry. Figure 8 shows the relation between the symmetry terms of the normal modes for the T_d, S_4, and C_s symmetries (see Supporting Information for graphical representations of the normal modes).

Normal-mode analysis of Mn^{IV}_4 compound - T_d symmetry

When an overall T_d symmetry for **1** is assumed, the 24 vibrational modes are divided into $2A_1$, 2E, $2T_1$, and $4T_2$ symmetry representations. Figure 8 shows that only the triply degenerate vibrational modes with T_2 symmetry are infrared active. As mentioned earlier we will concentrate only on the Mn–O stretching modes, which have the symmetry representations: A_1, E, T_1, and $2T_2$. Consequently, only two IR-active Mn–O stretching modes are anticipated. However, the IR absorption and difference spectra of the Mn^{IV}_4 compound show at least three strong absorption bands in Figure 3 at 510 cm^{-1}, 707 cm^{-1}, and 745 cm^{-1}. Nevertheless, a normal mode calculation was attempted to match two T_2 modes to these absorption bands. Table 1 presents a normal-mode analysis which assigns the 510 cm^{-1} and 745 cm^{-1} vibrational modes to the T_2 representation. The calculated values are similar to the observed values, including their isotopic shift. The mode at 707 cm^{-1} is assigned to the IR-inactive T_1 representation. However, this mode becomes partially active when the T_d symmetry breaks down, as shown in Figure 8.

Normal-mode analysis of Mn^{IV}_4 compound - S_4 symmetry

When the symmetry of the bpea ligand is included, the T_2 degenerate levels of the T_d symmetry split into the two IR-active E and B representations (Figure 8). Additionally, other vibrational modes become IR active in the S_4 symmetry. One absorption is derived from the T_1 symmetry representation, which splits into an IR-active doubly degenerate transition (symmetry representation E) and a Raman-active transition (symmetry representation A). The other new IR absorption comes from the degenerate E symmetry representation, and separates into an IR- (symmetry representation B) and a Raman- (symmetry representation A) active vibration.

Table 1 presents the results of the normal-mode analysis, assuming S_4 symmetry. The vibrational modes are organized as for T_d symmetry. The calculated values are similar to the observed values, including their isotopic shift. The 745 cm^{-1} feature is calculated to be an absorption band consisting of three vibrational modes; one at 743 cm^{-1} and two at 748 cm^{-1}. This splitting in the T_2 representation is supported by the broad bandwidth of ~20 cm^{-1} observed for this mode. A similar situation occurs for the 510 cm^{-1} mode, where the T_2 mode splits into one 489 cm^{-1} and two 506 cm^{-1} modes. Additionally, a new active mode in S_4 symmetry occurs at 512 cm^{-1}, which is derived from the E representation in T_d symmetry. This new band also contributes to the broad bandwidth of ~20 cm^{-1} observed for the 510 cm^{-1} mode. Therefore, the bandwidths of both the 510 cm^{-1} and 745 cm^{-1} are indications that a symmetry of S_4 or lower is required to explain the spectra of the Mn^{IV}_4 adamantane-like compound.

Table 1 indicates that the 707 cm^{-1} band is derived from the T_1 symmetry representation, as suggested earlier. When the overall S_4 symmetry is assumed, this band splits into an IR- and Raman-active doubly degenerate mode at 707 cm^{-1}, and a Raman-active mode at 705 cm^{-1}. This band has a bandwidth of about ~14 cm^{-1}, which suggests that the doubly degenerate mode has

split, indicating the distorted S_4 symmetry of the adamantane-like compound.

Normal-mode analysis of $Mn^{III}Mn^{IV}_3$ compound - C_s symmetry

The one-electron reduced compound **2** approaches an overall C_s symmetry when the symmetry of the bpea ligand is neglected. Figure 8 shows that all of the degeneracies are split upon reduction of **1** and all vibrational modes become IR and Raman active. Consequently, not only are shifts in peaks anticipated due to reduction of the compound, but also broadening of the previously degenerate modes, and new modes in the IR spectra, are expected.

The broad reversible difference signal at ~710 cm^{-1} resembles the signature of the (^{16}O – ^{18}O) difference spectrum of the solid Mn^{IV}_4 compound (Figure 4). However, unlike isotopic exchange, redox chemistry causes significant changes in bond lengths, bond angles, bond strengths, and consequently, the overall symmetry of the compound. This results in different frequency shifts for each vibrational mode, including possible shifts to higher energy. Owing to the change in overall symmetry, certain modes will become IR active or inactive, and the isotopic shifts will also alter. Therefore, simulating the difference signal in the 750 - 650 cm^{-1} and 520 - 460 cm^{-1} ranges is not straightforward.

To reduce the complexity of the normal mode calculations of **2** some additional assumptions about the force constants are necessary. The stretching force constants of all Mn^{IV}–O bonds are kept at the values calculated from the solid state spectrum of **1**, $f_{r^{IV}}$ = 3.10 mdyn/Å, and a Mn^{III}–O stretching force constant, $f_{r^{III}}$, is included. Introducing a second Mn^{III}–O force constant to account for Jahn-Teller distortion does not improve the fitting significantly. However, the Jahn-Teller distortion does have an significant effect on the kinetic energy matrix, which contains geometry and structural information. Hence this structural

information is included in the kinetic energy matrix for compound **2**. Two types of stretching coupling constants are used: with either oxygen, f_{rOr}, or manganese, f_{rMnr}, at the apex.

Using overall C_s symmetry and these force constant variables, the normal modes of **2** were calculated from the difference signals of the (Mn^{IV}_4–$Mn^{III}Mn^{IV}_3$) difference spectra and the (^{16}O – ^{18}O) double-difference spectrum (Figure 7). Four different objectives were sought with the normal mode calculation. The first objective was to try to simulate the difference signals in the 620 -720 cm^{-1} range for both the ^{16}O and ^{18}O spectra. The second objective was to match the (^{16}O – ^{18}O) double-difference signal in this range. The third objective was to simulate the difference signals in the 420 -520 cm^{-1} range for both the ^{16}O and ^{18}O spectra. The final objective was to obtain a simulation that matches the (^{16}O – ^{18}O) double-difference signal in this range, especially the positive signals around 510 cm^{-1} and 448 cm^{-1} and the negative band at 490 cm^{-1}.

Table 2 presents the calculated frequencies which gave a reasonable simulation of the difference and double-difference signals, as shown in Figure 9 (for graphical representations of the normal modes see Supporting Information). Normal-mode calculations give only the absorption frequencies of the normal modes; they do not give any information about the width or intensity of these transitions. Therefore, the intensities and bandwidths are based on the information that was obtained from the solid-state spectra. Figure 9 shows that the simulated spectra match the measured spectra reasonably well in the 620 -720 cm^{-1} range. There are small differences between frequencies and bandwidths, but the simulated spectra contain all of the observed features. The ^{18}O difference spectrum has the poorest match, which is due to the fact that the isotopic exchange is only 90% complete. Therefore, the ^{18}O difference spectrum also contains signals of adamantane-like compounds with various $^{16}O/^{18}O$ ratios, causing the observed

signal to be broader than the calculated one.

It was more difficult to match the simulated signals with the observed signals in the 425 - 520 cm^{-1} range. All of the vibrational modes undergo major changes upon reduction of **1**. Therefore, it is difficult to match all of the calculated changes with the observed shifts in this range. Nevertheless, the simulations match the observed spectra reasonably well, especially the double-difference spectrum (Figure 9). Only slight shifts in some of the normal modes are needed to improve the match between simulated and observed signals. This could be achieved by including more stretching force constants, such as a Jahn-Teller and a non-Jahn-Teller force constant for the Mn^{III}–O bond, or coupling force constants dependent on the oxidation state of the Mn atoms . However, including more variables will not give more significant information about the compound; and therefore, this expansion of variables is not presented.

Relevance to the Mn Cluster in the Oxygen Evolving Complex of Photosystem II

In summary, a good match is obtained (Tables 1 and 2) between the calculated vibrational frequencies, using reasonable assumptions about symmetry and force constants, and the observed vibrational modes, indicating that this approach is valid. Sheats et al.[62] used a similar approach to explain their results for a mono-μ-oxo bridged binuclear compound. One of the assumptions also made by Sheats et al.[62] is that the Mn–N interaction is much weaker than the μ-oxo bridge Mn–O interaction and hence can be excluded from the normal mode analysis. As mentioned in the introduction most of the ligands to the Mn-cluster are carboxylate groups. Some of these carboxylate groups may be bridging ligands between Mn atoms in the OEC, which will influence the Mn–O core modes. Therefore, these interactions may need to be included in the normal-mode analysis of the OEC.

Another influence on the bridging Mn–O interaction is the number of bridging oxygens to the Mn atom. As expected, the force constant of a Mn^{III}–O bond, $f_{r\,III}$ = 2.45 mdyn/Å, is weaker than that of the Mn^{IV}–O bond, $f_{r\,IV}$ = 3.10 mdyn/Å. However, both of these values are smaller than the value found for the Mn^{III}–O bond, $f_{r\,III}$ = 3.34 mdyn/Å, of the mono-μ-oxo compound $[Mn^{III}_2O(O_2CCH_3)_2(HB(pz)_3)_2]$ studied by Sheats et al.[62] This is an indication that the strength of the Mn–X bond depends not only on the oxidation state of Mn and the electronegativity of X, but also on the character of the other bridging ligands. The manganese atoms in the adamantane-like compound have three μ-oxo bridge oxygens. Most likely, the number of μ-oxo bridges influences the strength of the Mn–O bonds. Therefore, it is imperative that more manganese compounds are studied to provide further insight into the behavior of these Mn–O vibrational modes and to provide more accurate models of the OEC.

The IR spectra of the oxidized compound **1** in both the solid state and in solution show three distinct bands at about 510, 707 and 745 cm^{-1}, which are assigned to the asymmetric Mn–O–Mn stretching modes. The Mn–O–Mn mode at 707 cm^{-1} shifts by 33 cm^{-1} on isotopic substitution (^{16}O with ^{18}O) of the bridging mono μ-oxo group. The vibrational bands at 510 and 745 cm^{-1} are downshifted by 20 and 40 cm^{-1} respectively on ^{18}O substitution. These isotopic shifts are well calculated by the normal mode analysis. The magnitude of this shift of the Mn–O–Mn bridging frequency is typical of the downshift observed in di-μ-oxo bridged binuclear Mn compounds where both the bridges are substituted by ^{18}O.[49,56] These shifts were confirmed by normal-mode analysis (data not shown). In the only other study with a binuclear mono-μ-oxo-bridged Mn compound where ^{16}O was replaced by ^{18}O, the downshift was from 717 to 680 cm^{-1}; a downshift of 37 cm^{-1} that compares well with our study.[62]

A seminal FTIR difference study of the Mn cluster in the oxygen evolving complex by

Babcock and coworkers has identified an IR band at 606 cm^{-1} with the Mn–O–Mn stretching mode.[52] The band at 606 cm^{-1} shifts downward by only about 10 cm^{-1} on isotopic substitution, in contrast to the ~30 cm^{-1} shift seen in the di-μ-oxo compounds in other studies ([49] and references therein) and in the mono-μ-oxo bridged complex shown in this study. The small shift was attributed to partial substitution of only one of the di-μ-oxo bridges of a Mn_2O_2 unit; an explanation based on the observation of a 9 cm^{-1} shift in a di-μ-oxo bridged Mn compound with about 53% isotopic replacement.[23] However, other explanations are possible, such as the presence of a hydroxo bridged group, or a hydrogen bonding network that leads to the smaller shift on ^{18}O substitution in the OEC.

On reduction of a Mn^{IV} to Mn^{III} in the electrochemical cycle of the adamantane-like compound, we observe a shift in the most intense band from 709 to 680 cm^{-1}, a shift of 29 cm^{-1}, and in the band at 510 to 493 cm^{-1}, a shift of 17cm^{-1}. There is no shift in the third band observed at 745 cm^{-1} on reduction. All three bands are also sensitive to isotopic substitution; shifting from 680 to 653, 493 to 471 and 745 to 705 cm^{-1} on reduction in the ^{18}O compound. The shifts of 17 and 29 cm^{-1} observed on reduction in this study are in contrast to the two other studies that have probed the effect of oxidation or reduction on the Mn–O–Mn bridging vibrational bands in di-μ-oxo bridged binuclear Mn complexes.[23,56] Dave and coworkers[56] report a 1 cm^{-1} downward shift on oxidation ($Mn_2^{III,IV}$ to $Mn_2^{IV,IV}$), while the study by Cooper and coworkers[23] reports a upward shift of about 6 cm^{-1} on oxidation. We are unaware of any other IR study using a mono-μ-oxo bridged binuclear Mn complex , with Mn oxidation states of +3 or +4. Vincent and coworkers[76] reported that there are major changes in the vibrational frequencies of carboxylate groups (~1400 – 1700 cm^{-1}, note these are not Mn–O bands) bridged between Mn atoms on change in

oxidation state from Mn^{III} to Mn^{IV}. The shifts reported were as large as 100 cm^{-1}. The shifts we observe are in accord with what one expects from a change in the oxidation state of the metal ion, that would be caused by a change in the force constant of the Mn–O bond involved due to a change in the Mn oxidation state change. It is very surprising, however, that we observe such a major shift on the change in the oxidation state of only one Mn atom out of four. These results clearly point to what one can expect from the OEC and also the difficulties involved in assigning the vibrational modes involved, as explained below.

In contrast, for the oxygen-evolving complex of PS II the IR band, assigned as the Mn–O–Mn normal mode, is identified as shifting from 625 to 606 cm^{-1} during the S_1 to S_2 transition;[52] a downward shift for a transition that is supposed to correspond to a Mn^{III} to Mn^{IV} oxidation.[5] As detailed above, with the compound that we investigated there was a major change in symmetry that would theoretically make all 12 bridging Mn–O–Mn modes IR active. However, we observed only three of these bands and it is also possible that the bands observed in the oxidized compound are not the same modes observed in the reduced species (see Supporting Information). The change in symmetry makes it possible that one can observe other modes. Hence, the tacit assumption that the band shifts from 625 to 606 cm^{-1} during the S_1 and S_2 transition maybe an oversimplification. Because of changes in symmetry upon oxidation, as seen in the adamantane-like compound, it is possible that the two bands are not the same vibrational modes and are from entirely different symmetry representations (this can be seen also in the Supporting Information). The data from the present study show that it is too simplistic to look for one-to-one correspondence in bands on oxidation or reduction when this entails a change in symmetry of the molecule.

The disparities between the OEC and the trends seen in the adamantane-like compound

could also be due to a difference in Mn–O core structure; from EXAFS it is known that the adamantane-like compound spectra do not match the PS II data.[3-5,77,78] Additionally, half of the ligands to the Mn atoms in the adamantane-like compound are N-ligands and half are O-ligands, while the majority of the Mn ligands in the OEC are O-ligands.[10,15,39] The character of the ligands to the Mn atoms influences the Mn–O bond strengths and consequently the vibrational modes. Therefore, one could expect to observe differences in IR spectra between the adamantane-like compound and the OEC, even if the Mn–O cores are structurally the same.

From the normal mode analysis it is known that the adamantane-like compound has 24 vibrational stretching modes. The overall symmetry determines whether all of these vibrational modes are IR active. However, even when all modes are dipole-allowed, their intensities may be weak. In case of compound **1** and **2**, only one strong, well-resolved absorption band is observed at 707 cm^{-1} or 680 cm^{-1}, and a broad absorption band at 745 cm^{-1}. Various weaker absorption bands occur in the 520-425 cm^{-1} range, even though some of these vibrations are dipole-allowed in the highest symmetry. This might explain why so far only one IR band has been observed for the OEC. It is possible that the intensities of the other modes are weak and cannot be observed with the current sensitivity. Alternatively not all modes may be IR active, depending on the overall symmetry of the OEC. It is important to observe the weaker vibrational modes of the OEC during the catalytic cycle to have an informative interpretation of the IR data. These bands might be easier to observe using Raman spectroscopy, as some might be formally allowed transitions. For example, in the case of compound **1** the A_1 mode in T_d symmetry is not observed because it is IR inactive, but this mode should be observed in the Raman spectrum.

Development of a novel spectroelectrochemical technique enabled us to study IR (oxidized minus reduced) difference solution spectra, with good signal-to-noise ratio and at low

concentrations of the adamantane-shaped $\{Mn_4O_6\}$ core. This method allowed us to study homologous compounds in different oxidation states, which are relevant to the catalytical cycle of the oxygen-evolving complex in photosystem II. These IR spectra and their analysis provide additional means for the interpretation of the vibrational modes of other model compounds, as well as for the OEC.

Acknowledgements

The authors would like to thank Dr. Heinz Frei for the use of the Bruker IFS88 FTIR spectrometer. This research was supported by the Director, Office of Science, Office of Basic Energy Sciences, Division of Energy Biosciences, U.S. Department of Energy under contract DE-AC03-76SF00098 and by the National Institutes of Health grant (GM 55302).

Supporting Information available: Graphical representation of the vibrational normal modes of the adamantane-like compound

Tables

Table 1 Comparison of the observed and calculated frequencies for the $[Mn^{IV}_4O_6(bpea)_4]^{4+}$ compound. The observed IR frequencies are of the solid compounds in KBr pellets (see also Fig. 3). The optimal force constants are given for an overall T_d or S_4 symmetry: $f_{r^{IV}}$ = 3.15 mdyn/Å, f_{rOr} = 0.55 mdyn/Å, and f_{rMnr} = 0.20 mdyn/Å in case of T_d symmetry, or $f_{r^{IV}}$ = 3.10 mdyn/Å, f_{rOr} = 0.50 mdyn/Å, and f_{rMnr} = 0.20 mdyn/Å in case of S_4 symmetry. (For graphical representations of the normal modes see Supporting Information.)

Symmetry		^{16}O (cm^{-1})			^{18}O (cm^{-1})			Δ (cm^{-1})		
T_d	S_4	Obs.	Calc.		Obs.	Calc.		Obs.	Calc.	
			T_d	S_4		T_d	S_4		T_d	S_4
$2T_2$	B	745	746	743	705	709	706	40	37	37
	E			748			711			37
	B	510	508	489	490	492	473	20	16	16
	E			506			490			16
T_1	A	707	706	705	674	673	672	33	33	33
	E			707			673			34
E	A	–	511	504	–	496	487	–	15	17
	B			512			497			15
A_1	A	–	503	491	–	485	474	–	18	17

Table 2 Comparison of the observed and calculated frequencies for the $[Mn^{III}Mn^{IV}_3O_6(bpea)_4]^{3+}$ compound. The observed IR frequencies of the Mn–O modes are of the electrochemical solution. Overall C_s symmetry is assumed. Bending force constants are set at zero, and stretching force constants are: $f_{r^{IV}}$ = 3.10 mdyn/Å, $f_{r^{III}}$ = 2.45 mdyn/Å, f_{rOr} = 0.40, and f_{rMnr} = 0.15 mdyn/Å. The normal modes are organized as for T_d in Table 1. (For graphical representations of the normal modes see Supporting Information.)

C_s	^{16}O (cm^{-1})		^{18}O (cm^{-1})		Δ (cm^{-1})	
	Obs.	Calc.	Obs.	Calc.	Obs.	Calc.
2A'	~745	747, 709	~705	710, 674	~40	37, 35
A"		747		710		37
2A'	493	492, 478	471	476, 463	22	16, 15
A"		464		449		15
A'	680	685	653	653	27	32
2A"		726, 689		692, 656		34, 33
A'	–	505	–	488	–	17
A"		500		485		15
A'	–	466	–	450	–	16

Figure Captions

Figure 1 The adamantane-like manganese compound $[Mn^{IV}_4O_6(bpea)^4]^{4+}$, with the non-aromatic nitrogen of each bpea ligand indicated by an asterisk.

Figure 2 Schematic of the data-collection protocol used to obtain the (Mn^{IV}_4 – $Mn^{III}Mn^{IV}_3$) difference spectra. Each experiment contains 2 full redox cycles that consists of 5 redox steps. During the first redox step (labeled 1) no potential is applied, i.e. spectra are taken of the compound in the oxidized state. The first step is followed by four redox steps by alternating reducing (labeled 2 and 4) and oxidizing potentials (labeled 3 and 5) applied to the solution. This protocol enables us to obtain four spectra from two complete redox cycles. Only the maxima and minima of the oscillating IR intensity are used to calculate the difference spectra from the oxidation (2 minus 3, and 4 minus 5) and reduction cycles (1 minus 2, and 3 minus 4), indicated by the thicker lines in the schematic. The difference spectra from the oxidation cycle are multiplied by –1, so that for both redox steps the signals due to the Mn^{IV}_4 species are positive and negative for the $Mn^{III}Mn^{IV}_3$ species. Consequently, reversible features have the same sign in the difference spectra during both the reduction and oxidation cycles, and non-reversible features have the opposite sign. Therefore, when the averaged difference spectra from the reduction and oxidation cycle are added the non-reversible background signals are eliminated and only the reversible features remain in the Sum spectrum. The Sum spectra are calculated by adding a fraction, *a*, of the averaged difference spectrum during the oxidation cycle from the difference spectrum during the reduction cycle, with the objective of minimizing the irreversible signals in the

Sum spectrum over the whole 400 - 4000 cm^{-1} range.

Figure 3 The FTIR absorption spectra of the solid $[Mn^{IV}_4\mathbf{^{16}O}_6(bpea)_4]^{4+}$ (black) and $[Mn^{IV}_4\mathbf{^{18}O}_6(bpea)_4]^{4+}$ (red) compounds in KBr pellets, at a resolution of 1 cm^{-1}, average of 100 scans. The FTIR ($^{16}O - {}^{18}O$) difference spectrum (blue) is obtained by minimizing the contribution of the bpea modes. Arrows indicate frequencies of major difference peaks between the two isotopic spectra.

Figure 4 Simulation of the ($^{16}O - {}^{18}O$) FTIR difference signal around 700 cm^{-1} of the $[Mn^{IV}_4O_6(bpea)_4]^{4+}$ compound (blue line), fitted with four gaussian absorption curves (black and red lines, green is the sum of the gaussian curves). The two positive black gaussian curves represent the absorption bands of the ^{16}O species at 745 cm^{-1} and 707 cm^{-1}, with bandwidths at half height of 20 cm^{-1} and 14 cm^{-1}, respectively. The two negative red curves are the companion modes of the ^{18}O species at 705 cm^{-1} and 674 cm^{-1}, with bandwidths and intensity identical to those of the ^{16}O gaussians curves.

Figure 5 The FTIR (oxidized – reduced) difference spectra of a 2.8 mM $[Mn^{IV}_4\mathbf{^{16}O}_6(bpea)_4]^{4+}$ 0.1 M TBA(PF_6) acetonitrile solution. The Sum spectrum (black) is the sum of the averaged difference spectrum from the reduction cycle (purple) and the averaged difference spectrum from the oxidation cycle (blue). The details are explained in the methods and materials and in the caption for Figure 2. Irreversible signals due to decomposition of the electrolyte solution are indicated by ‡, and those due to changes in counter ion PF_6^- concentration are indicated by *. Reversible signals are indicated by black and red arrows; the red arrows indicate signals sensitive to the $^{16}O \rightarrow {}^{18}O$ isotopic exchange (see Figure 6). Positive reversible signals are due to the Mn^{IV}_4 oxidation state, and negative signals due to the $Mn^{III}Mn^{IV}_4$ oxidation state.

Figure 6 The FTIR (oxidized – reduced) difference spectra of a 2.5 mM $[Mn^{IV}_4\mathbf{^{18}O}_6(bpea)_4]^{4+}$ 0.1 M TBA(PF_6) acetonitrile solution. The Sum spectrum (black) is the sum of the averaged difference spectrum from the reduction cycle (purple) and the averaged difference spectrum from the oxidation cycle (blue). The details are explained in the methods and materials and in the caption for Figure 2. Irreversible signals due to decomposition of the electrolyte solution are indicated by ‡, and those due to changes in counter ion PF_6^- concentration are indicated by *. Reversible signals are indicated by black and red arrows, with the red arrows marking sensitivity to the $^{16}O \rightarrow {}^{18}O$ isotopic exchange (see Figure 5). Positive reversible signals are due to the Mn^{IV}_4 oxidation state, and negative signals due to the $Mn^{III}Mn^{IV}_4$ oxidation state.

Figure 7 The FTIR (oxidized – reduced) difference spectra of the ^{16}O (black) and ^{18}O (red) species, and the (^{16}O – ^{18}O) double-difference spectrum (blue). The red arrows indicate the two regions sensitive to $^{16}O \rightarrow {}^{18}O$ exchange. Irreversible signals due decomposition of the electrolyte solution are indicated by ‡, and those due to changes in counter ion PF_6^- concentration are indicated by *.

Figure 8 The relation among the overall symmetry representations of the Mn compound which were used for the analysis of the two oxidation states. When the influence of the terminal ligand, bpea, on the compound is ignored, the T_d and the C_s symmetry apply to the $Mn^{IV}{}_4$ and $Mn^{III}Mn^{IV}{}_3$ compounds, respectively. When the influence of bpea on the compound is included the S_4 symmetry applies to the $Mn^{IV}{}_4$ species. IR and R indicate whether a symmetry term is infrared or Raman active.

Figure 9 A comparison of the observed ^{16}O (black) and ^{18}O (red) (oxidized-reduced) difference spectra and the (^{16}O – ^{18}O) double-difference spectrum (blue) with the simulated spectra (green). The simulated spectra are obtained using the calculated frequencies of S_4 symmetry for the $Mn^{IV}{}_4$ species, Table 1, and C_s symmetry for the $Mn^{III}Mn^{IV}{}_3$ species, Table 2. The arrows indicate the frequencies that were optimized. Irreversible signals due to the counter ion PF_6^- are indicated by *.

References

(1) Kok, B.; Forbush, B.; McGloin, M. *Photochem. Photobiol.* **1970**, *11*, 457-475.

(2) Zouni, A.; Witt, H. T.; Kern, J.; Fromme, P.; Krauss, N.; Saenger, W.; Orth, P. *Nature* **2001**, *409*, 739-743.

(3) Penner-Hahn, J. E. *Struct. Bonding (Berlin)* **1998**, *90*, 1-36.

(4) Robblee, J. H.; Cinco, R. M.; Yachandra, V. K. *Biochim. Biophys. Acta* **2001**, *1503*, 7-23.

(5) Yachandra, V. K.; Sauer, K.; Klein, M. P. *Chem. Rev.* **1996**, *96*, 2927-2950.

(6) Dismukes, G. C.; Siderer, Y. *Proc. Natl. Acad. Sci. USA* **1981**, *78*, 274-278.

(7) Messinger, J.; Robblee, J. H.; Yu, W. O.; Sauer, K.; Yachandra, V. K.; Klein, M. P. *J. Am. Chem. Soc.* **1997**, *119*, 11349-11350.

(8) Miller, A. F.; Brudvig, G. W. *Biochim. Biophys. Acta* **1991**, *1056*, 1-18.

(9) Peloquin, J. M.; Britt, R. D. *Biochim. Biophys. Acta* **2001**, *1503*, 96-111.

(10) Debus, R. J. *Biochim. Biophys. Acta* **1992**, *1102*, 269-352.

(11) Hillier, W.; Messinger, J.; Wydrzynski, T. *Biochemistry* **1998**, *37*, 16908-16914.

(12) Hillier, W.; Wydrzynski, T. *Biochim. Biophys. Acta* **2001**, *1503*, 197-209.

(13) Messinger, J.; Badger, M.; Wydrzynski, T. *Proc. Natl. Acad. Sci. U. S. A.* **1995**, *92*, 3209-3213.

(14) Noguchi, T.; Sugiura, M. *Biochemistry* **2000**, *39*, 10943-10949.

(15) Debus, R. J. In *Manganese and Its Role in Biological Processes*; Sigel, A., Sigel, H., Eds.; Marcel Dekker, Inc.: New York, 2000; Vol. 37, pp 657-711.

(16) Messinger, J.; Robblee, J. H.; Bergmann, U.; Fernandez, C.; Glatzel, P.; Visser, H.; Cinco, R. M.; McFarlane, K. L.; Bellacchio, E.; Pizarro, S. A.; Cramer, S. P.; Sauer, K.; Klein, M. P.; Yachandra, V. K. *J. Am. Chem. Soc.* **2001**, *123*, 7804-7820.

(17) Roelofs, T. A.; Liang, M. C.; Latimer, M. J.; Cinco, R. M.; Rompel, A.; Andrews, J. C.; Sauer, K.; Yachandra, V. K.; Klein, M. P. *Proc. Natl. Acad. Sci. U. S. A.* **1996**, *93*, 3335-3340.

(18) Ono, T.; Noguchi, T.; Inoue, Y.; Kusunoki, M.; Matsushita, T.; Oyanagi, H. *Science* **1992**, *258*, 1335-1337.

(19) Iuzzolino, L.; Dittmer, J.; Dörner, W.; Meyer-Klaucke, W.; Dau, H. *Biochemistry* **1998**, *37*, 17112-17119.

(20) Christou, G. *Acc. Chem. Res.* **1989**, *22*, 328-335.

(21) Armstrong, W. H. In *Manganese Redox Enzymes*; Pecoraro, V. L., Ed.; VCH Publishers: New York, 1992; pp 261-286.

(22) Cinco, R. M.; Rompel, A.; Visser, H.; Aromí, G.; Christou, G.; Sauer, K.; Klein, M. P.; Yachandra, V. K. *Inorg. Chem.* **1999**, *38*, 5988-5998.

(23) Cooper, S. R.; Calvin, M. *J. Am. Chem. Soc.* **1977**, *99*, 6623-6630.

(24) Pecoraro, V. L.; Baldwin, M. J.; Gelasco, A. *Chem. Rev.* **1994**, *94*, 807-826.

(25) Pecoraro, V. L.; Hsieh, W.-Y. In *Manganese and Its Role in Biological Processes*; Sigel, A., Sigel, H., Eds.; Marcel Dekker Inc.: New York, 2000; Vol. 37, pp 429-504.

(26) Visser, H.; Anxolabéhère-Mallart, E.; Bergman, U.; Glatzel, P.; Robblee, J. H.; Cramer, S. P.; Girerd, J.-J.; Sauer, K.; Klein, M. P.; Yachandra, V. K. *J. Am. Chem. Soc.* **2001**, *123*, 7031-7039.

(27) Wieghardt, K. *Angew. Chem.-Int. Edit. Engl.* **1989**, *28*, 1153-1172.

(28) Limburg, J.; Brudvig, G. W.; Crabtree, R. H. In *Biomimetic oxidations catalyzed by transition metal complexes*; Meunier, B., Ed.; Imperial College Press: London, 2000; pp 509-541.

(29) Ruettinger, W. F.; Campana, C.; Dismukes, G. C. *J. Am. Chem. Soc.* **1997**, *119*, 6670-6671.

(30) Haumann, M.; Junge, W. *Biochim. Biophys. Acta* **1999**, *1411*, 86-91.

(31) Hoganson, C. W.; Babcock, G. T. In *Manganese and Its Role in Biological Processes*; Sigel, A., Sigel, H., Eds.; Marcel Dekker Inc.: New York, 2000; Vol. 37, pp 613-656.

(32) Messinger, J. *Biochim. Biophys. Acta* **2000**, *1459*, 481-488.

(33) Renger, G. *Biochim. Biophys. Acta* **2001**, *1503*, 210-228.

(34) Tommos, C.; Babcock, G. T. *Acc. Chem. Res.* **1998**, *31*, 18-25.

(35) Kambara, T.; Govindjee *Proc. Natl. Acad. Sci. U. S. A.* **1985**, *82*, 6119-6123.

(36) Dau, H.; Iuzzolino, L.; Dittmer, J. *Biochim. Biophys. Acta* **2001**, *1503*, 24-39.

(37) Kuzek, D.; Pace, R. J. *Biochim. Biophys. Acta* **2001**, *1503*, 123-137.

(38) Siegbahn, P. E. M.; Crabtree, R. H. *J. Am. Chem. Soc.* **1999**, *121*, 117-127.

(39) Vrettos, J. S.; Limburg, J.; Brudvig, G. W. *Biochim. Biophys. Acta* **2001**, *1503*, 229-245.

(40) Nugent, J. H. A.; Rich, A. M.; Evans, M. C. W. *Biochim. Biophys. Acta* **2001**, *1503*, 138-146.

(41) Brudvig, G. W.; Beck, W. F.; De Paula, J. C. *Annu. Rev. Biophys. Biophys. Chem.* **1989**, *18*, 25-46.

(42) Christou, G.; Vincent, J. B. *Biochim. Biophys. Acta* **1987**, *895*, 259-274.

(43) Chu, H.-A.; Hillier, W.; Law, N. A.; Sackett, H.; Haymond, S.; Babcock, G. T. *Biochim. Biophys. Acta* **2000**, *1459*, 528-532.

(44) Noguchi, T.; Inoue, Y.; Tang, X. S. *Biochemistry* **1999**, *38*, 10187-10195.

(45) Noguchi, T.; Ono, T. A.; Inoue, Y. *Biochim. Biophys. Acta* **1993**, *1143*, 333-336.

(46) Noguchi, T.; Ono, T. A.; Inoue, Y. *Biochim. Biophys. Acta* **1995**, *1232*, 59-66.

(47) Steenhuis, J. J.; Barry, B. A. *J. Phys. Chem. B* **1997**, *101*, 6652-6660.

(48) Steenhuis, J. J.; Hutchison, R. S.; Barry, B. A. *J. Biol. Chem.* **1999**, *274*, 14609-14616.

(49) Chu, H. A.; Hillier, W.; Law, N. A.; Babcock, G. T. *Biochim. Biophys. Acta* **2001**, *1503*, 69-82.

(50) Chu, H.-A.; Debus, R. J.; Babcock, G. T. *Biochemistry* **2001**, *40*, 2312-2316.

(51) Chu, H.-A.; Gardner, M. T.; O'Brien, J. P.; Babcock, G. T. *Biochemistry* **1999**, *38*, 4533-4541.

(52) Chu, H.-A.; Sackett, H.; Babcock, G. T. *Biochemistry* **2000**, *39*, 14371-14376.

(53) Fischer, G.; Wydrzynski, T. *J. Phys. Chem. B* **2001**, *105*, 12894-12901.

(54) Cua, A.; Stewart, D. H.; Reifler, M. J.; Brudvig, G. W.; Bocian, D. F. *J. Am. Chem. Soc.* **2000**, *122*, 2069-2077.

(55) Cooper, S. R.; Dismukes, G. C.; Klein, M. P.; Calvin, M. *J. Am. Chem. Soc.* **1978**, *100*, 7248-7252.

(56) Dave, B. C.; Czernuszewicz, R. S. *Inorg. Chim. Acta* **1994**, *227*, 33-41.

(57) Dave, B. C.; Czernuszewicz, R. S. *Inorg. Chim. Acta* **1998**, *281*, 25-35.

(58) Davidson, G. *Spectroscopic Properties of Inorganic and Organo-mettalic Compounds*; The Royal Society of Chemmistry, U.K.: London, 1997; Vol. 30.

(59) Nakamoto, K. *Infrared and Raman Specra of Inorganic and Coordination Compounds*; 5th ed.; John Wiley & Sons: New York, 1997.

(60) Ross, S. D. *Inorganic Infrared and Raman Spectra*; McGraw-Hill: London, 1972.

(61) Baldwin, M. J.; Stemmler, T. L.; Riggs-Gelasco, P. J.; Kirk, M. L.; Penner-Hahn, J. E.; Pecoraro, V. L. *J. Am. Chem. Soc.* **1994**, *116*, 11349-11356.

(62) Sheats, J. E.; Czernuszewicz, R. S.; Dismukes, G. C.; Rheingold, A. L.; Petrouleas, V.; Stubbe, J.; Armstrong, W. H.; Beer, R. H.; Lippard, S. J. *J. Am. Chem. Soc.* **1987**, *109*, 1435-1444.

(63) Gonzalez-Vilchez, F.; Griffith, W. P. *J.C.S. Dalton Trans.* **1972**, 1416-1421.

(64) Varetti, E. L.; Filgueira, R. R.; Müller, A. *Spectrochim. Acta* **1981**, *37A*, 369-373.

(65) Varetti, E. L.; Müller, A. *Z. anorg. allg. Chem.* **1978**, *422*, 230-234.

(66) Edwards, H. G. M.; Ware, M. J.; Woodward, L. A. *Chem. Commun.* **1968**, 540-541.

(67) Edwards, H. G. M.; Woodward, L. A.; Gall, M. J.; Ware, M. J. *Spectrochim. Acta, Part A* **1970**, *26*, 287-290.

(68) Czernuscewicz, R. S.; Su, Y. O.; Stern, M. K.; Macor, K. A.; Kim, D.; Groves, J. T.; Spiro, T. G. *J. Am. Chem. Soc.* **1988**, *110*, 4158-4165.

(69) Dubé, C. E.; Wright, D. W.; Pal, S.; Bonitatebus, P. J.; Armstrong, W. H. *J. Am. Chem. Soc.* **1998**, *120*, 3704-3716.

(70) Wieghardt, K.; Bossek, U.; Gebert, W. *Angew. Chem.-Int. Edit. Engl.* **1983**, *22*, 328-329.

(71) Visser, H.; Curtright, A. E.; McCusker, J. K.; Sauer, K. *Anal. Chem.* **2001**, *73*, 4374-4378.

(72) Milosevic, M.; Sting, D.; Rein, A. *Spectroscopy* **1995**, *10*, 44-49.

(73) Sheridan, R. E.; Rein, A. J. *R&D* **1991**, *33*, 100-102.

(74) Visser, H. PhD thesis, University of California, Berkeley, **2001,** LBNL-47934.

(75) Wilson, E. B.; Decius, J. C.; Cross, P. C. *Molecular Vibrations: The Theory of Infrared and Raman Vibrational Spectra*; Dover Publications, Inc.: New York, 1955.

(76) Smith, J. C.; Gonzalez-Vergara, E.; Vincent, J. B. *Inorg. Chim. Acta* **1997**, *255*, 99-103.

(77) Liang, W.; Roelofs, T. A.; Cinco, R. M.; Rompel, A.; Latimer, M. J.; Yu, W. O.; Sauer, K.; Klein, M. P.; Yachandra, V. K. *J. Am. Chem. Soc.* **2000**, *122*, 3399-3412.

(78) DeRose, V. J.; Mukerji, I.; Latimer, M. J.; Yachandra, V. K.; Sauer, K.; Klein, M. P. *J. Am. Chem. Soc.* **1994**, *116*, 5239-5249.

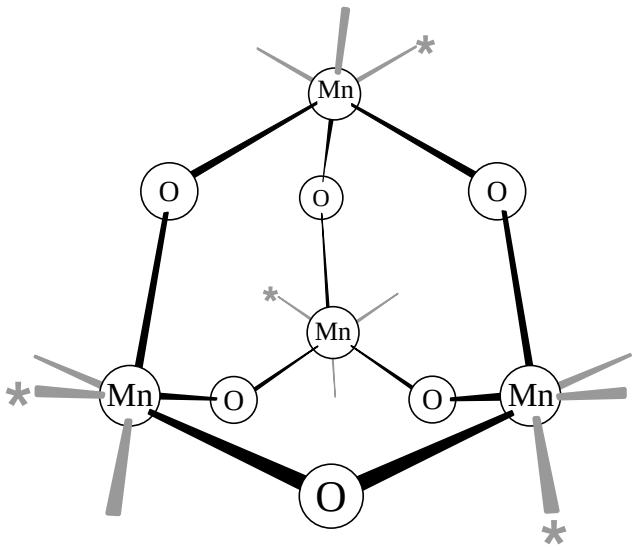

bpea =

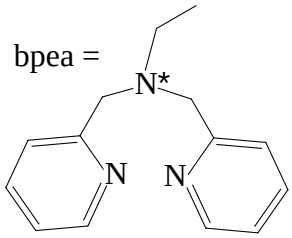

Figure 1

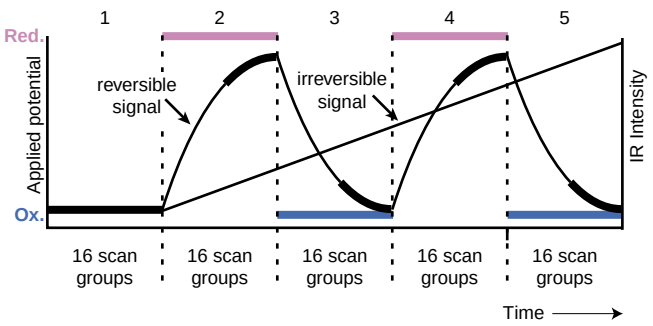

Reduction cycle difference spectra
(1 – 2)
(3 – 4)

Oxidation cycle difference spectra
– (2 – 3)
– (4 – 5)

Sum spectra = (Av. Red. cycle diff. spectra) + a x (Av. Ox. cycle diff. spectra)

Figure 2

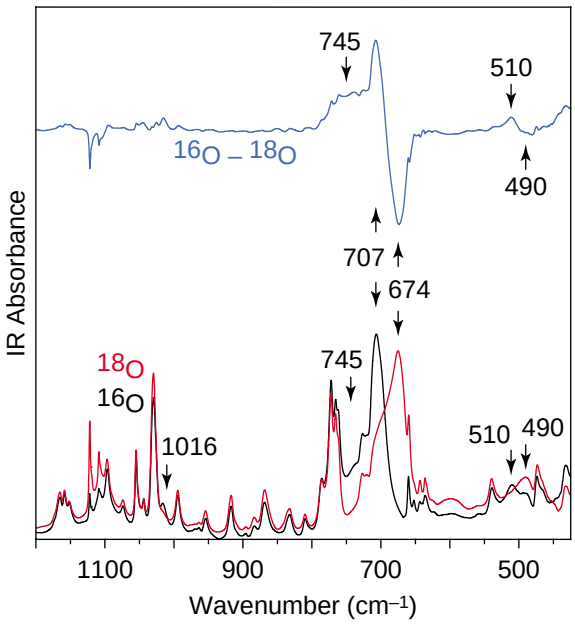
745
510
16O – 18O
490
707
674
IR Absorbance
18O
16O
745
1016
510
490
1100
900
700
500
Wavenumber (cm–1)

Figure 3

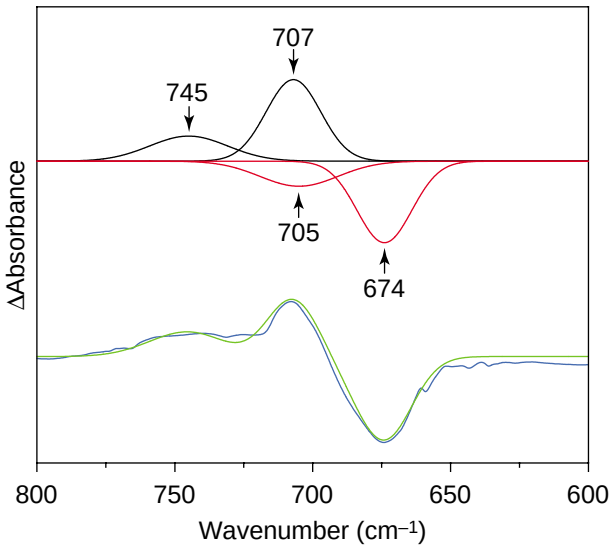
707
745
705
674
ΔAbsorbance
800
750
700
650
600
Wavenumber (cm⁻¹)

Figure 4

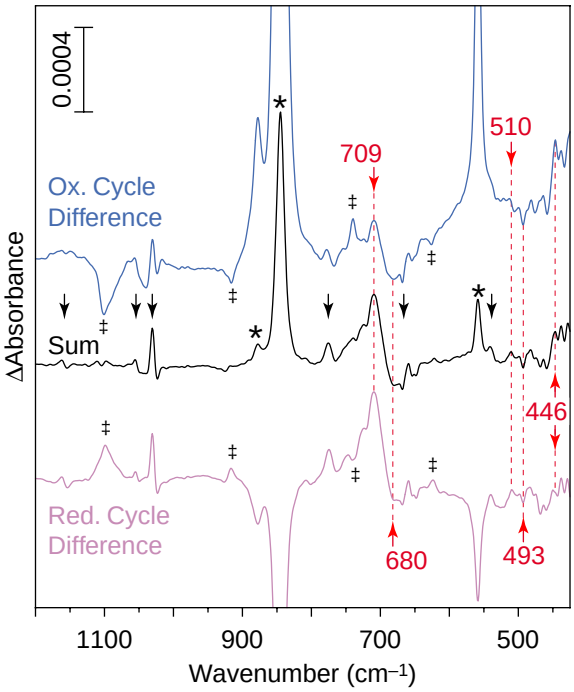
0.0004
Ox. Cycle
Difference
Sum
Red. Cycle
Difference
ΔAbsorbance
709
510
446
680
493
1100
900
700
500
Wavenumber (cm⁻¹)

Figure 5

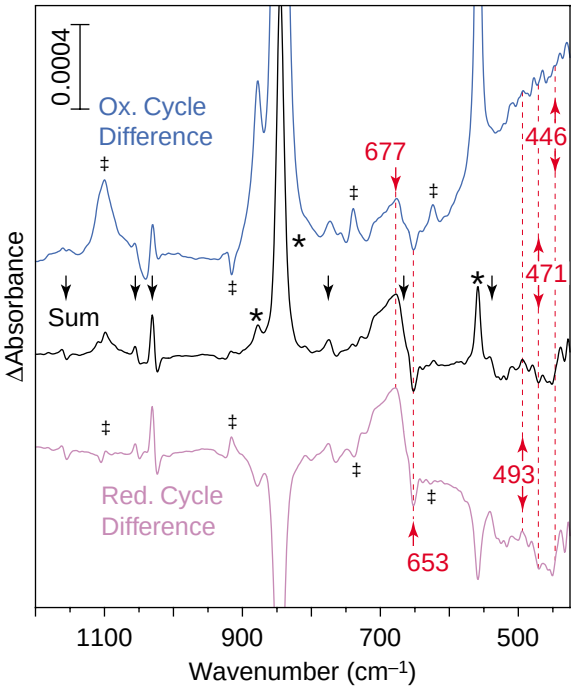
0.0004
Ox. Cycle
Difference
677
446
471
Sum
493
Red. Cycle
Difference
653
ΔAbsorbance
1100
900
700
500
Wavenumber (cm⁻¹)

Figure 6

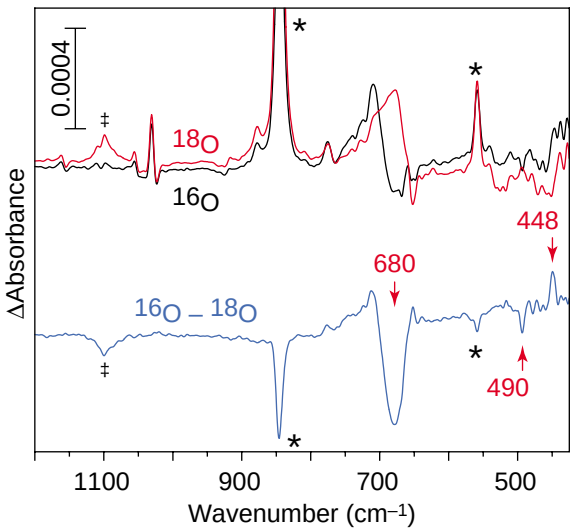
0.0004
‡
18O
16O
*
*
448
680
16O – 18O
*
490
‡
*
ΔAbsorbance
1100
900
700
500
Wavenumber (cm–1)

Figure 7

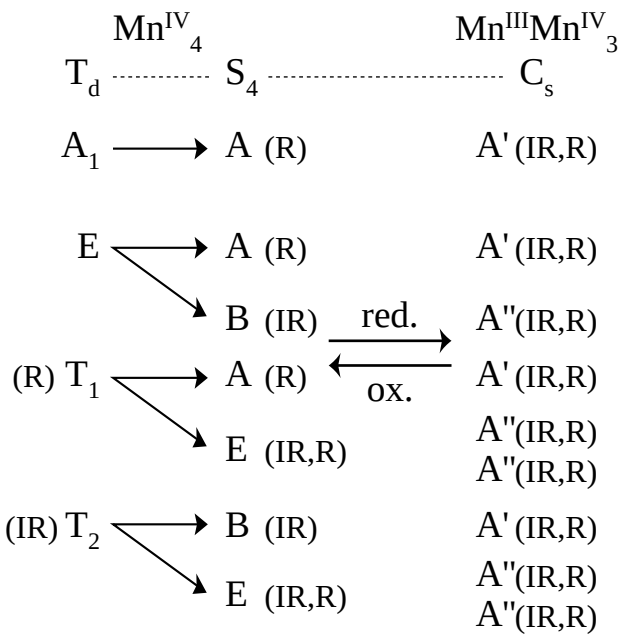
Mn^IV_4
Mn^III Mn^IV_3
T_d
S_4
C_s
A_1
A (R)
A' (IR,R)
E
A (R)
A' (IR,R)
B (IR)
red.
A" (IR,R)
(R) T_1
A (R)
ox.
A' (IR,R)
E (IR,R)
A" (IR,R)
A" (IR,R)
(IR) T_2
B (IR)
A' (IR,R)
E (IR,R)
A" (IR,R)
A" (IR,R)

Figure 8

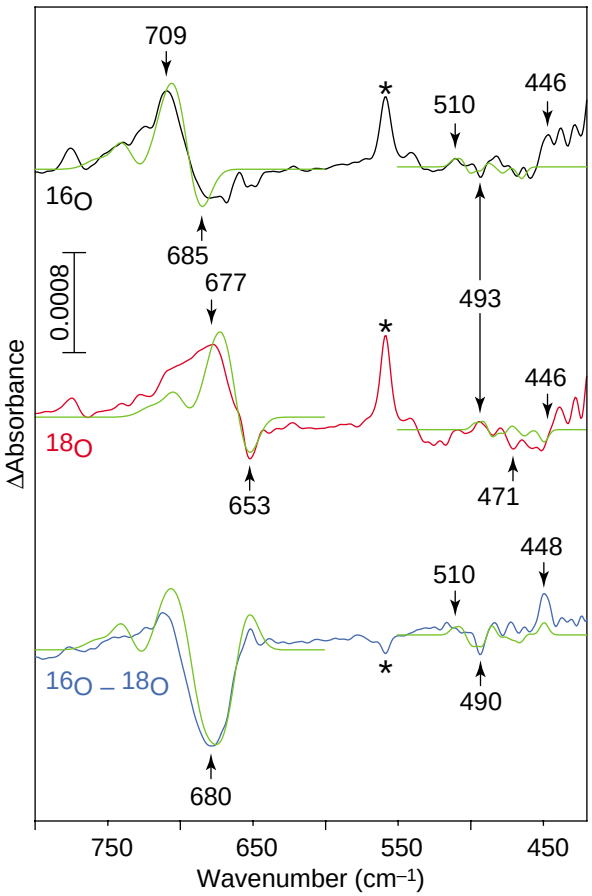
709
*
510
446
16O
685
0.0008
677
493
*
446
18O
653
471
448
510
16O – 18O
*
490
680
750
650
550
450
Wavenumber (cm–1)
ΔAbsorbance

Figure 9

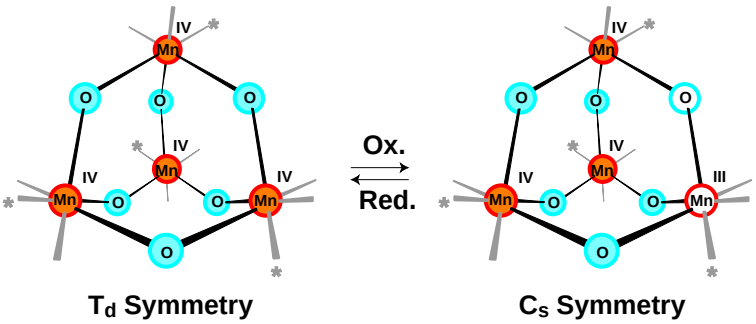

T_d Symmetry

C_s Symmetry

Table of Content Figure